

Path-integral calculation of the third dielectric virial coefficient of helium based on *ab initio* three-body polarizability and dipole surfaces

Giovanni Garberoglio,^{1,2, a)} Allan H. Harvey,^{3, b)} Jakub Lang,^{4, c)} Michał Przybytek,^{4, d)} Michał Lesiuk,^{4, e)} and Bogumił Jeziorski^{4, f)}

¹⁾ *European Centre for Theoretical Studies in Nuclear Physics and Related Areas (FBK-ECT*), Trento, I-38123, Italy.*

²⁾ *Trento Institute for Fundamental Physics and Applications (INFN-TIFPA), via Sommarive 14, 38123 Trento, Italy*

³⁾ *Applied Chemicals and Materials Division, National Institute of Standards and Technology, Boulder, CO 80305, USA.*

⁴⁾ *Faculty of Chemistry, University of Warsaw, Pasteura 1, 02-093 Warsaw, Poland.*

(Dated: 7 August 2024)

We develop a surface for the electric dipole moment of three interacting helium atoms and use it, together with state-of-the-art potential and polarizability surfaces, to compute the third dielectric virial coefficient, C_ε , for both ^4He and ^3He isotopes. Our results agree with previously published data computed using an approximated form for the three-body polarizability, and are extended to the low-temperature regime by including exchange effects. Additionally, the uncertainty of C_ε is rigorously determined for the first time by propagating the uncertainties of the potential and polarizability surfaces; this uncertainty is much larger than the contribution from the dipole-moment surface to C_ε . Our results compare reasonably well with the limited experimental data. The first-principles values of C_ε computed in this work will enhance the accuracy of primary temperature and pressure metrology based on measurements of the dielectric constant of helium.

I. INTRODUCTION

Primary metrology for pressure and thermodynamic temperature has been transformed in recent years by the ability to make precise electrical, optical, and acoustic measurements on noble gases. Examples include dielectric-constant gas thermometry,^{1–3} refractive-index gas thermometry,^{4–7} acoustic gas thermometry,⁸ and *ab initio* pressure standards based on dielectric measurements.^{9,10}

The use of helium gas for such standards is particularly attractive, because the small number of electrons makes it possible to compute properties of atoms, pairs of atoms, and to some extent triplets of atoms with extremely small uncertainties, much smaller than can be obtained from experiment.¹¹ An example is the static polarizability of the ^4He atom, which has been computed with a relative standard uncertainty near 1×10^{-7} (0.1 ppm).¹²

For dielectric-based standards, the dielectric virial coefficients are essential quantities. These coefficients appear in the expansion around the zero-density limit of the Clausius–Mossotti function in powers of molar density ρ :

$$\frac{\varepsilon - 1}{\varepsilon + 2} = \rho (A_\varepsilon + B_\varepsilon \rho + C_\varepsilon \rho^2 + \dots), \quad (1)$$

where ε is the static dielectric constant and A_ε is proportional to the mean static polarizability of the isolated molecule. B_ε is the second dielectric virial coefficient, C_ε is the third dielectric virial coefficient, etc. These virial coefficients are functions of the thermodynamic temperature T .

The second dielectric virial coefficient $B_\varepsilon(T)$ depends only on the pair potential and the interaction-induced pair polarizability; for helium the former has been calculated with extremely high accuracy¹³ and the latter is also fairly well known.¹⁴ Garberoglio and Harvey computed B_ε of helium, along with the related second refractivity virial coefficient, with full accounting for quantum effects.¹⁵ The expanded ($k = 2$) uncertainty in B_ε was only $0.2 \text{ cm}^6 \text{ mol}^{-2}$ at most temperatures, increasing to $0.4 \text{ cm}^6 \text{ mol}^{-2}$ as the temperature decreased to 1 K. At temperatures near 273 K, this is less than 0.5% in relative terms.

Calculation of the third dielectric virial coefficient $C_\varepsilon(T)$ is much more complex. Recently, three of us¹⁶ presented the first complete framework for calculation of C_ε , making use of a path-integral Monte Carlo (PIMC) method to fully account for quantum effects. In addition to the pair quantities required for B_ε , this calculation requires multidimensional surfaces for the three-body non-additive potential energy, for the three-body non-additive polarizability, and for the dipole moment of a three-atom configuration. Because surfaces were not available for the three-body polarizability and dipole moment, Garberoglio *et al.*¹⁶ approximated them with simple expressions valid in the limit of large interatomic distances, so their calculated results were not rigorous and lacked uncertainty estimates. In the meantime, a

^{a)} Corresponding author: garberoglio@ectstar.eu

^{b)} Electronic mail: allan.harvey@nist.gov

^{c)} Electronic mail: jakub.lang@chem.uw.edu.pl

^{d)} Electronic mail: m.przybytek@uw.edu.pl

^{e)} Electronic mail: m.lesiuk@uw.edu.pl

^{f)} Deceased

fully *ab initio* three-body polarizability surface has been developed¹⁷ and the non-additive three-body potential¹⁸ has been improved.

In this work, we present the dipole-moment surface of an assembly of three helium atoms, provide a brief review of the theoretical framework for calculating C_ε , and use the developed dipole-moment surface, together with the latest three-body potential and polarizability, to compute C_ε , with uncertainty estimates, from 1 K to 3000 K. We compare our calculations to the limited (and scattered) experimental data available for this quantity, noting that the uncertainties in our calculated $C_\varepsilon(T)$ are much smaller than those of the experimental data.

II. THREE-BODY DIPOLE SURFACE

For three interacting atoms located at fixed positions in space specified by vectors \mathbf{r}_i , $i \in \{1, 2, 3\}$, the electric dipole moment $\mathbf{m}(\mathbf{r}_1, \mathbf{r}_2, \mathbf{r}_3)$ is defined as a vector

$$m_\alpha(\mathbf{r}_1, \mathbf{r}_2, \mathbf{r}_3) = - \left. \frac{\partial \mathcal{E}(\mathbf{r}_1, \mathbf{r}_2, \mathbf{r}_3, \mathbf{E})}{\partial E_\alpha} \right|_{\mathbf{E}=0}, \quad (2)$$

where $\alpha \in \{x, y, z\}$ and $\mathcal{E}(\mathbf{r}_1, \mathbf{r}_2, \mathbf{r}_3, \mathbf{E})$ is the electronic energy in the presence of a static and uniform electric field \mathbf{E} with components E_α . As the dipole moment of atoms and homonuclear diatoms vanishes, $\mathbf{m}(\mathbf{r}_1, \mathbf{r}_2, \mathbf{r}_3)$ for a system of three interacting helium atoms is effectively equal to its three-body component $\mathbf{m}_3(\mathbf{r}_1, \mathbf{r}_2, \mathbf{r}_3)$. This observation allows us to remove the basis set superposition error (BSSE)¹⁹ from the calculated dipole moments using the complete counterpoise correction,²⁰ which has been shown to be applicable not only in the calculations of interaction energies^{19–21} but also for interaction-induced dipole moments and polarizabilities.^{17,22} The counterpoise corrected three-body dipole moment $\mathbf{m}_3(\mathbf{r}_1, \mathbf{r}_2, \mathbf{r}_3)$ is obtained by combining results from seven separate calculations,

$$\begin{aligned} \mathbf{m}_3(\mathbf{r}_1, \mathbf{r}_2, \mathbf{r}_3) &= \mathbf{m}(\mathbf{r}_1, \mathbf{r}_2, \mathbf{r}_3)_B \\ &\quad - \mathbf{m}(\mathbf{r}_1, \mathbf{r}_2)_B - \mathbf{m}(\mathbf{r}_2, \mathbf{r}_3)_B - \mathbf{m}(\mathbf{r}_1, \mathbf{r}_3)_B \\ &\quad + \mathbf{m}(\mathbf{r}_1)_B + \mathbf{m}(\mathbf{r}_2)_B + \mathbf{m}(\mathbf{r}_3)_B, \end{aligned} \quad (3)$$

where $\mathbf{m}(\mathbf{r}_1, \mathbf{r}_2, \mathbf{r}_3)_B$ is the dipole moment of the full trimer, $\mathbf{m}(\mathbf{r}_i, \mathbf{r}_j)_B$ is the dipole moment of the diatom comprising atoms located at \mathbf{r}_i and \mathbf{r}_j , and $\mathbf{m}(\mathbf{r}_i)_B$ is the dipole moment of the i -th atom. All contributions on the right-hand side of Eq. (3) are computed using the same basis set B of the trimer. Note that, due to the presence of basis functions located on all three atomic centers, the diatomic dipole moments $\mathbf{m}(\mathbf{r}_i, \mathbf{r}_j)_B$ are not necessarily zero and depend on the position of the third atom. Analogously, the atomic dipole moments $\mathbf{m}(\mathbf{r}_i)_B$ depend on the position of the other two atoms. The contributions $\mathbf{m}(\mathbf{r}_i, \mathbf{r}_j)_B$ and $\mathbf{m}(\mathbf{r}_i)_B$ vanish only in the complete basis set limit.

Before delving into computational details, we first analyze the accuracy requirements in calculation of the

three-body dipole moment of helium from the point of view of the present work. Note that the contribution of the three-body dipole moment to the third dielectric virial coefficient is expected to be small in comparison with the three-body polarizability, especially for higher temperatures. In fact, the three-body dipole moment enters the calculations through the factor $|\mathbf{m}_3|^2/(k_B T)$ and, additionally, the square of the three-body dipole moment, $|\mathbf{m}_3|^2$, is smaller by one to two orders of magnitude than the corresponding value of the isotropic three-body polarizability (when both quantities are expressed in atomic units). Taking into consideration that the average uncertainty in the best theoretical results currently available in the literature for the three-body polarizability is of the order of several percent, uncertainties larger by a factor of ten in the three-body dipole moment are still acceptable.

We performed *ab initio* calculations of the three-body dipole moment of helium for 734 atomic configurations defined in terms of interatomic distances r_{12} , r_{23} , and r_{13} that satisfy the triangle inequality. This set contains a subset of configurations used in Ref. 17 (600 points), obtained by excluding equilateral and centrosymmetric linear configurations for which the dipole moment vanishes by symmetry. The additional points were generated using the incremental procedure described in Sec. III.B of Ref. 17 and Sec. 3.2 of Ref. 18. If necessary, the interatomic distances defining initial configurations were relabeled to ensure that they are sorted according to their magnitude, that is, $r_{12} \leq r_{23} \leq r_{13}$. In this case, the angle θ_2 at the vertex corresponding to atom 2, which can be calculated from the law of cosines as

$$\theta_2 = \arccos \frac{r_{12}^2 + r_{23}^2 - r_{13}^2}{2r_{12}r_{23}}, \quad (4)$$

necessarily satisfies the condition $\theta_2 \geq \pi/3$. During the calculations, the atoms were assumed to lie in the xy -plane with atoms 1 and 2 placed along the x -axis. With this choice, the z component of the dipole moment is equal to zero for all configurations.

The dipole moments were calculated using the CC3 method²³ as implemented in the Dalton 2018 package.^{24,25} We used tight convergence criteria, between 10^{-7} and 10^{-10} depending on the geometry, for the coupled-cluster ground state and response functions iterations, as molecular properties tend to be sensitive to such thresholds. In general, for smaller interatomic distances it is more difficult to achieve convergence and the thresholds were looser in such cases. Nonetheless, at least four significant digits are stable in the results for all geometries of the trimer.

The calculations were performed using a family of doubly augmented correlation-consistent Gaussian basis sets, referred to further as dXZ, where X is the cardinal number. These basis sets were developed in Ref. 26 specifically to accurately describe interactions of helium atoms in their ground state. The most important difference between the dXZ basis sets and the standard Dunning's

TABLE I. Basis set convergence of the length of the three-body dipole moment $|\mathbf{m}_3|$ of helium calculated at the CC3 level of theory using the dXZ family of basis sets. The interatomic distances, r_{ij} , are in units of a_0 and the electric dipole moment is in units of $10^{-3} e a_0 \approx 8.478354 \times 10^{-33}$ C m.

r_{12}	r_{23}	r_{13}	$X = 2$	$X = 3$	$X = 4$	$X = 5$	$X = 6$
3.01	7.28	8.96	0.066435	0.064043	0.063199	0.062926	0.062791
3.91	4.41	6.76	0.130613	0.118156	0.114890	0.114201	0.113865
4.40	5.88	8.23	0.013709	0.011621	0.011066	0.010938	0.010891
4.51	5.78	9.97	0.012897	0.012214	0.011845	0.011791	0.011757
3.07	4.97	4.97	0.280883	0.303940	0.304889	0.304283	0.303943
7.56	10.94	12.06	0.000003	0.000012	0.000013	0.000014	0.000014
7.56	12.06	15.44	0.000003	0.000009	0.000010	0.000010	0.000010

d-aug-cc-pVXZ basis sets for helium^{27,28} is that in the former the augmenting functions, optimized to accurately reproduce the asymptotic expansion of the pair potential, are more diffuse (have smaller exponents) than in the latter, especially for angular momenta $l \geq 2$. Therefore, the dXZ basis sets are more suitable for calculations of molecular properties, such as the dipole moment and polarizability, that require proper description of the electronic wave function at large distances from the nuclei.

The largest basis set of this family which is currently available is d6Z. Unfortunately, calculations within the d6Z basis are possible only for a handful of configurations due to the enormous computational costs. Nonetheless, we obtained d6Z results for a few configurations in order to test the basis set convergence of the calculated data. This allows us to select the basis which yields sufficient accuracy at minimal possible cost.

In Table I, we present the results obtained for several representative configurations. For a vast majority of configurations, the d4Z values are essentially converged and are very close to the d5Z and d6Z results. For example, for the isosceles configuration with side lengths $(r_{12}, r_{23}, r_{13}) = (3.07 a_0, 4.97 a_0, 4.97 a_0)$, where $a_0 \approx 52.91772105$ pm is the atomic unit of length, we ob-

serve a difference of only 0.3% between the d4Z and d6Z basis sets. According to the above discussion, such error is negligible in the present context. A similar behavior is found for other tested geometries, see Table I. As a consequence, we recommend to use the results obtained with d4Z basis set for all 734 configurations. While calculations within the d5Z basis for 734 configurations would be feasible with our resources, we expect them to be at least an order of magnitude more costly than for d4Z. In the face of minuscule accuracy improvement offered by the d5Z basis, as demonstrated in Table I, we refrained from its use for the whole surface.

To create an analytic representation of the surface of $|\mathbf{m}_3|^2$, we developed a model function expressed as a sum of a short-range part and a long-range part. The short-range part contains a factor which forces it to vanish for equilateral and centrosymmetric linear configurations. When the interatomic distances are sorted as described above, such configurations correspond to the situation where $r_{12} = r_{23}$ and θ_2 is equal to either $\pi/3$ or π , respectively. The long-range part of the fitting function is a sum of squares of properly symmetrized expressions for the long-range expansion of the x - and y -components of the dipole moment taken from the work of Li and Hunt.²⁹ The complete model function has the following form

$$\begin{aligned}
 |\mathbf{m}_3|^2 = & \left[|r_{12} - r_{23}| + (1 - 2 \cos \theta_2)(1 + \cos \theta_2) \right] \sum_{l=1}^6 e^{-\alpha_l r_{12} - \beta_l r_{23}} \sum_{\substack{0 \leq i \leq j \leq k \leq 5 \\ i+j+k \leq 7}} A_{ijk,l} r_{12}^i r_{23}^j (1 + \cos k \theta_2) \\
 & + \sum_{\alpha \in \{x,y\}} \left[S_{123} \left(D_d \frac{3R_{12,\alpha} \cos \theta_2 + R_{23,\alpha}}{r_{12}^3 r_{23}^7} f_3(r_{12}) f_7(r_{23}) + D_q \frac{R_{12,\alpha}(5 \cos^2 \theta_2 - 1) + 2R_{23,\alpha}}{r_{12}^4 r_{23}^6} f_4(r_{12}) f_6(r_{23}) \right) \right]^2, \quad (5)
 \end{aligned}$$

where α_l , β_l , and $A_{ijk,l}$ are the fitting parameters, S_{123} denotes the operator that symmetrizes the expression it precedes with respect to the variables \mathbf{r}_1 , \mathbf{r}_2 , and \mathbf{r}_3 , $R_{ij,\alpha} = r_{i,\alpha} - r_{j,\alpha}$, $f_n(x)$ are the Tang–Toennies damping functions³⁰

$$f_n(x) = 1 - e^{-x} \left(1 + x + \frac{x^2}{2!} + \dots + \frac{x^n}{n!} \right), \quad (6)$$

and D_d and D_q are the asymptotic constants.

Several estimates of the the asymptotic constants D_d and D_q were reported in the literature. Bruch *et al.*³¹ provided $D_d = -25.70$ and $D_q = -5.18$ using pseudospectral representation of the dipole and quadrupole operators. Somewhat different values were calculated by Li and Hunt,²⁹ $D_d = -21.63$ and $D_q = -4.36$, from the dipole and quadrupole integrals obtained by Fowler³² through

TABLE II. Comparison of the absolute relative percentage deviation, $|\mathbf{m}_3|_{\text{asympt}} - |\mathbf{m}_3|_{\text{calc}}|/|\mathbf{m}_3|_{\text{calc}} \times 100\%$, of the asymptotic expansion for the dipole moment calculated using asymptotic constants from Ref. 31 ($D_d = -25.70$, $D_q = -5.18$) and from Ref. 29 ($D_d = -21.63$, $D_q = -4.36$) with respect to the *ab initio* results calculated as CC3[d4Z] and ^sFCI[d4Z] (see text for definitions). Interatomic distances r_{ij} are in units of a_0 .

r_{12}	r_{23}	r_{13}	CC3[d4Z]		^s FCI[d4Z]	
			Ref. 31	Ref. 29	Ref. 31	Ref. 29
8.012274	8.012274	13.5	1.06%	14.94%	7.03%	21.75%
8.309025	8.309025	14.0	1.39%	17.00%	9.08%	23.48%
8.605776	8.605776	14.5	2.68%	18.09%	10.14%	24.37%
8.902527	8.902527	15.0	3.22%	18.55%	10.57%	24.73%
9.199278	9.199278	15.5	3.33%	18.64%	10.63%	24.79%
9.496029	9.496029	16.0	3.14%	18.48%	10.31%	24.51%
9.792780	9.792780	16.5	2.79%	18.19%	10.05%	24.29%
10.089531	10.089531	17.0	2.35%	17.82%	9.68%	23.98%
10.386282	10.386282	17.5	2.26%	17.73%	9.61%	23.93%
10.683033	10.683033	18.0	1.38%	17.00%	8.82%	23.26%
10.979784	10.979784	18.5	0.92%	16.61%	8.41%	22.92%
11.276534	11.276534	19.0	0.47%	16.22%	8.02%	22.58%
11.573285	11.573285	19.5	0.05%	15.88%	7.65%	22.28%

the coupled Hartree–Fock (CHF) method. Li and Hunt also provided alternative estimates of the D_d constant, $D_d = -25.63$ and $D_d = -25.4$, using pseudospectral calculations of the dipole integrals from the works of Bishop and Pipin³³ and Whisnant and Byers Brown,³⁴ respectively. However, the corresponding D_q constants were not given. Martin³⁵ used a simple approximation to the resolvents based on the calculations for hydrogen atoms and obtained $D_d = -18.54$ and $D_q = -3.70$. However, the last results are most likely not accurate enough for our purposes and are not considered in the following discussion.

To determine which set of asymptotic constants is consistent with our *ab initio* results for the dipole moment, in Table II we compare our results obtained for isosceles geometries with large sides with the long-range expansion calculated using asymptotic constants from the papers of Bruch *et al.*³¹ and Li and Hunt.²⁹ However, one has to be careful in such direct comparison – while our results are well-saturated with respect to the basis set size, higher-order excitations not included in the CC3 model are still missing. Therefore, there is a possibility of accidental agreement between two sets of results. To eliminate such possibility, we compare the long-range expansions not only with our CC3 data, but also with an estimate of the FCI results derived from our calculations. Similarly as at the CC3 level of theory, we expect the FCI results to be converged with the basis set size already in the d4Z basis. The FCI result in the d4Z basis is estimated by a simple scaling procedure employing results from the a3Z basis set¹⁷ as follows

$${}^s\text{FCI}[\text{d4Z}] = \text{CC3}[\text{d4Z}] \times \frac{\text{FCI}[\text{a3Z}]}{\text{CC3}[\text{a3Z}]}, \quad (7)$$

where $M[B]$ denotes a result obtained using method M with basis set B and ^sFCI[d4Z] is the approximation to the FCI result with the d4Z basis set. Raw *ab initio* results CC3[d4Z] for all 734 configurations considered in this work, and CC3[a3Z] and FCI[a3Z] results for configurations from Table II are given in the Supplementary Material.

When the asymptotic constants from Bruch *et al.*³¹ are used in the asymptotic expansion, a good agreement with the CC3 dipole moments is observed, see Table II. The constants estimated by Li and Hunt²⁹ lead to worse agreement with CC3, with discrepancies of the order of 15% or more. Crucially, similar trends are observed when comparing with the FCI estimates. When the higher excitations are included, the differences between the asymptotic expansion and *ab initio* data rise to about 8–10% in case of the constants from Bruch *et al.*³¹ The constants from Li and Hunt²⁹ result in differences on the order of 22–25%. Overall, for all isosceles geometries with large sides (the smallest interatomic distance is $9.0 a_0$), the mean absolute relative deviation of the asymptotic expansions from the *ab initio* data is 5% when the asymptotic constants from Bruch *et al.*³¹ are used and about 20% while using the constants from Li and Hunt.²⁹ For these reasons, the asymptotic constants D_d and D_q from Bruch *et al.*³¹ were used in the model function, Eq. (5), in all subsequent calculations.

Similar analysis as in the previous paragraph can be used to estimate the uncertainty of our calculation due to missing higher-order excitations. Based on the analysis presented in Table II, and similar for other configurations, we assumed a very conservative estimation of the uncertainty of our *ab initio* data to be equal to 30% of the recommended values. This estimation is intended to take into account the basis set incompleteness error, the uncertainty of the value of the asymptotic constants, and the missing contribution of the higher electronic excitations. We believe that it is reasonable to interpret this estimated uncertainty as an expanded ($k = 2$) uncertainty, roughly corresponding to a 95% confidence interval.

After fixing the D_d and D_q constants, the remaining parameters in Eq. (5) were fitted using the Levenberg–Marquardt algorithm as implemented in the SciPy package.³⁶ During the optimization, the linear parameters (for fixed values of the nonlinear ones) were obtained using the weighted linear least-squares minimization with weights equal to inverse of estimated uncertainty squared. The mean relative error of the fit is 23% with a median equal to 12% with respect to the recommended values of the magnitude of the dipole moment squared. In the Supplementary Material we provide the optimized parameters of the fitting function (5) along with a FORTRAN code for its evaluation.

III. AB INITIO CALCULATION OF DIELECTRIC VIRIAL COEFFICIENTS

The theoretical framework enabling the *ab initio* calculation of the dielectric virial coefficients appearing in the generalized Clausius–Mossotti equation (1) has been developed in Ref. 16. In this section, we will briefly recall the most important results and describe the details of the calculations reported below.

Denoting by $Q_N(V, T, E_0)$ the partition function of N particles in a volume V at temperature T and in the presence of an electric field E_0 generated by sources external to the volume V , and defining the reduced partition functions

$$\frac{Z_N(T, E_0)}{N!} = \frac{Q_N(V, T, E_0) V^N}{Q_1(V, T, E_0)^N}, \quad (8)$$

the dielectric virial coefficients appearing in Eq. (1) are given by

$$B_\epsilon = \frac{2\pi k_B T}{3V} \frac{\partial^2 Z_2(V, T, E_0)}{\partial E_0^2}, \quad (9)$$

$$C_\epsilon = -\frac{2\pi k_B T}{3} \left[\frac{2}{V^2} \left(\frac{\partial Z_2}{\partial E_0} \right)^2 + \frac{2(Z_2 - V^2)}{V^2} \frac{\partial^2 Z_2}{\partial E_0^2} - \frac{1}{3V} \left(\frac{\partial^2 Z_3}{\partial E_0^2} - 3V \frac{\partial^2 Z_2}{\partial E_0^2} \right) \right], \quad (10)$$

where the derivatives with respect to the external electric field are to be evaluated in the limit $E_0 \rightarrow 0$. In this work, we will be concerned with the third dielectric virial coefficient, $C_\epsilon(T)$ of Eq. (10). In the general case of quantum statistical mechanics, one can write³⁷

$$Q_N(V, T, E_0) = \frac{1}{N!} \sum_{i, \sigma} \langle i | e^{-\beta H(N)} \mathcal{P}_\sigma | i \rangle, \quad (11)$$

where $\beta = 1/(k_B T)$, σ runs over the permutations of N objects, and \mathcal{P}_σ is the corresponding operator in the Hilbert space of N particles, which includes the sign of the permutation in the case of fermions. The sum over i in Eq. (11) runs over all the eigenstates of the Hamiltonian $H(N)$, which can be in turn expressed as $H(N) = H_0(N) + \Delta H_{\mathbf{m}}(N) + \Delta H_{\boldsymbol{\alpha}}(N)$ where

$$H_0(N) = \sum_{i=1}^N \frac{\pi_i^2}{2m} + \sum_{i<j} u_2(i, j) + \sum_{i<j<k} u_3(i, j, k) + \dots \quad (12)$$

$$\Delta H_{\mathbf{m}}(N) = - \left(\sum_{i=1}^N \mathbf{m}_1(i) + \sum_{i<j} \mathbf{m}_2(i, j) + \sum_{i<j<k} \mathbf{m}_3(i, j, k) + \dots \right) \cdot \mathbf{E}_0 \quad (13)$$

$$\Delta H_{\boldsymbol{\alpha}}(N) = - \frac{1}{2} \mathbf{E}_0 \cdot \left(\sum_{i=1}^N \boldsymbol{\alpha}_1(i) + \sum_{i<j} \boldsymbol{\alpha}_2(i, j) + \sum_{i<j<k} \boldsymbol{\alpha}_3(i, j, k) + \dots \right) \cdot \mathbf{E}_0. \quad (14)$$

In Eqs. (12)–(14), m denotes the mass of the atoms, π is the momentum operator, and $u_k(1, \dots, k)$, $\mathbf{m}_k(1, \dots, k)$ and $\boldsymbol{\alpha}_k(1, \dots, k)$ are the k -body potential, dipole moment, and polarizability, respectively. Notice that the polarizabilities are 3×3 matrices.

In this work, we used for u_2 the pair potential developed by Czachorowski *et al.*,¹³ while u_3 is given by the three-body potential developed by Lang *et al.*¹⁸ We further used the pair polarizability $\boldsymbol{\alpha}_2$ by Cencek *et al.*¹⁴ and the three-body polarizability by Lang *et al.*¹⁷ All of these quantities come with rigorous uncertainty estimates. In the case of noble gases, the first non-zero dipole-moment contribution in Eq. (13) comes from the term \mathbf{m}_3 , which was determined for this work and is reported in Sec. II. Effects beyond the nonrelativistic Born–Oppenheimer approximation result in the interaction among ³He atoms being slightly different than that among ⁴He atoms. This has been taken into account in the case of the pair potential,¹³ but neglected for other quantities since the effect of the isotopic difference is negligible compared to other uncertainties.

For fluids like helium, where quantum effects are significant, the evaluation of $C_\epsilon(T)$ from Eq. (10), using Eqs. (8) and (11), is most conveniently performed using the path-integral formulation of quantum statistical mechanics.^{16,38,39} In this approach, one can show that the reduced partition functions Z_N can be evaluated as classical partition functions of an equivalent system, where each of the N atoms is substituted by a ring polymer with P monomers. The equivalence is exact in the $P \rightarrow \infty$ limit, although convergence of the results is usually obtained with a finite value of P , which is generally larger the lower the temperature considered. Additionally, the formalism provides a well-defined interaction law between the ring polymers corresponding to the various atoms, which depends on the actual interaction potentials $u_k(1, \dots, k)$; successive monomers interacts with a harmonic potential, with a spring constant that depends on T and P , as well as on the atomic mass and temperature. Physically, the size of the polymers is proportional to the thermal de Broglie wavelength of the atoms, $\Lambda = h/\sqrt{2\pi m k_B T}$, and takes into account quantum diffraction effects due to the uncertainty principle. Classical many-particles configurations obtained using the coordinates of monomers with the same index p ($1 \leq p \leq P$) are usually called an “imaginary-time slice”. Exchange effects due to particle indistinguishability are taken into account by considering coalesced ring polymers according to the specific permutation appearing in Eq. (11). As discussed in Refs. 16 and 39, the 6 possible permutations of 3 particles appearing in the sum of σ in Eq. (11) can be divided into three classes. The first class, with only one element, is the identity permutation, which corresponds to Boltzmann statistics (that is, distinguishable particles), and that will be denoted by the symbol \cdot . The second class includes the three permutations where only one pair is exchanged, and will be denoted by \cdot . Finally, the third class includes the two

cyclic permutations and we will denote it by Δ . In the case of two particles, one has only the identity (\cdot) and the pair permutation (\parallel). As a consequence, one can write

$$Z_3 = Z_3^\cdot + Z_3^\parallel + Z_3^\Delta \quad (15)$$

$$Z_2 = Z_2^\cdot + Z_2^\parallel, \quad (16)$$

$$C_\varepsilon^\cdot(T) = \frac{2\pi}{3} \int \left[\frac{1}{3} \left\langle \left(\frac{\beta |\overline{\mathbf{m}_3^\cdot}|^2}{3} + \overline{A_3^\cdot} \right) e^{-\beta \overline{V_3^\cdot}} - \sum_{i < j} \overline{\alpha_{\text{iso}}^\cdot(\mathbf{r}_{ij})} e^{-\beta \overline{V_2^\cdot}(\mathbf{r}_{ij})} \right\rangle - 2 \langle e^{-\beta \overline{V_2^\cdot}(\mathbf{r}_{21})} - 1 \rangle \langle \overline{\alpha_{\text{iso}}^\cdot(\mathbf{r}_{31})} e^{-\beta \overline{V_2^\cdot}(\mathbf{r}_{31})} \rangle \right] d\mathbf{r}_2 d\mathbf{r}_3, \quad (17)$$

$$C_\varepsilon^\parallel(T) = \frac{(-1)^{2I}}{2I+1} \frac{2\pi}{3} \frac{\Lambda^3}{2^{3/2}} \int d\mathbf{r} \left[\left\langle \left(\frac{\beta |\overline{\mathbf{m}_3^\parallel}|^2}{3} + \overline{A_3^\parallel} \right) e^{-\beta \overline{V_3^\parallel}} - \overline{\alpha_{\text{iso}}^\parallel} e^{-\beta \overline{V_2^\parallel}} \right\rangle - 2 \langle e^{-\beta \overline{V_2^\parallel}} \rangle \langle \overline{\alpha_{\text{iso}}^\parallel} e^{-\beta \overline{V_2^\parallel}} \rangle - 2 \langle \overline{\alpha_{\text{iso}}^\parallel} e^{-\beta \overline{V_2^\parallel}} \rangle \langle e^{-\beta \overline{V_2^\parallel}} - 1 \rangle \right] \quad (18)$$

$$C_\varepsilon^\Delta(T) = \frac{2\pi}{3} \frac{\Lambda^6}{(2I+1)^2} \left[\frac{2}{3^{5/2}} \left\langle \left(\frac{\beta |\overline{\mathbf{m}_3^\Delta}|^2}{3} + \overline{A_3^\Delta} \right) e^{-\beta \overline{V_3^\Delta}} \right\rangle - \frac{1}{4} \langle e^{-\beta \overline{V_2^\Delta}} \rangle \langle \overline{\alpha_{\text{iso}}^\Delta} e^{-\beta \overline{V_2^\Delta}} \rangle \right], \quad (19)$$

where we have denoted by I the nuclear spin of the atoms under consideration, that is $I = 0$ for ^4He and $I = 1/2$ for ^3He . The horizontal bars denote the average values of the various observables on the configurations in each imaginary-time slice of the ring polymers, whereas angular brackets denote the average over the possible internal configuration of polymers. In Eq. (17), the first monomer of one polymer is fixed at the origin of the coordinate system $\mathbf{r}_1 = 0$, the vectors \mathbf{r}_2 and \mathbf{r}_3 denote the position of the first monomer of the two polymers corresponding to the other two quantum particles and we have defined $\mathbf{r}_{ij} = \mathbf{r}_i - \mathbf{r}_j$. In Eq. (18), the vector \mathbf{r} points from the first monomer of the coalesced polymer to the first monomer of the particle unaffected by the permutation. The averages in Eq. (19) are obtained over the configuration of fully coalesced polymers of either three (Δ) or two (\parallel) particles.

The other quantities appearing in Eqs. (17)–(19) are: the isotropic component of the pair polarizability, $\alpha_{\text{iso}} = \text{tr}[\boldsymbol{\alpha}_2]/3$, the isotropic component of the full three-body polarizability

$$A_3(\mathbf{r}_{12}, \mathbf{r}_{13}, \mathbf{r}_{23}) = \text{tr}[\boldsymbol{\alpha}_3(\mathbf{r}_{12}, \mathbf{r}_{13}, \mathbf{r}_{23}) + \boldsymbol{\alpha}_2(\mathbf{r}_{12}, \mathbf{r}_{13}) + \boldsymbol{\alpha}_2(\mathbf{r}_{12}, \mathbf{r}_{23}) + \boldsymbol{\alpha}_2(\mathbf{r}_{13}, \mathbf{r}_{23})]/3, \quad (20)$$

the pair potential ($V_2 = u_2$) and the three-body potential $V_3(\mathbf{r}_{12}, \mathbf{r}_{13}, \mathbf{r}_{23}) = u_3(\mathbf{r}_{12}, \mathbf{r}_{13}, \mathbf{r}_{23}) + u_2(\mathbf{r}_{12}, \mathbf{r}_{13}) + u_2(\mathbf{r}_{12}, \mathbf{r}_{23}) + u_2(\mathbf{r}_{13}, \mathbf{r}_{23})$.

For details on how to sample the ring-polymer configurations corresponding to the various permutations, we refer to our original publications^{39–41} as well as the seminal papers by Fosdick and Jordan.^{42,43} In performing the calculations solving Eqs. (17)–(19), we used a temperature-dependent value of P , according to $P = \text{nint}(7 + 1600 \text{ K}/T)$ for ^4He and $P = \text{nint}(7 + 2000 \text{ K}/T)$ for ^3He , where $\text{nint}(x)$ denotes the nearest integer to x . For the convenience of calculation, we split the expres-

and, using Eq. (10), derive three contributions to the third dielectric virial coefficient¹⁶

sions for the various components of $C_\varepsilon(T)$ into five contributions, (roughly) in order of decreasing magnitude: the first, denoted by $C_\varepsilon^{\cdot, 2\text{-body}}$, is the Boltzmann contribution depending only on pair properties (that is, u_2 and $\boldsymbol{\alpha}_2$). The second term, denoted by, $C_\varepsilon^{\cdot, \text{diff-3}2}$, is the Boltzmann contribution that takes into account the difference between the dielectric virial coefficient calculated with the non-additive three-body potential and polarizability and $C_\varepsilon^{\cdot, 2\text{-body}}$. The two following contributions are the odd and even exchange contributions $-C_\varepsilon^\parallel$ and C_ε^Δ , respectively – from Eqs. (18) and (19). These four terms are computed neglecting the contribution of the three-body dipole-moment surface. The remainder, which we denote by $C_\varepsilon^{\text{dip}}$, takes into account all the terms where the dipole-moment surface \mathbf{m}_3 appears explicitly in both the Boltzmann and exchange contributions. This approach was found to be convenient in the calculation of density virial coefficients because the difference terms, which depend on the computationally demanding three-body surfaces, can be evaluated with an accuracy comparable to that of the two-body term by sampling a smaller number of Monte Carlo configurations. Notice that $C_\varepsilon^{\text{dip}}$ depends on the average of the directions of the dipole moment across the ring-polymer beads. However, the dipole-moment surface developed here, Eq. (5), provides only the squared modulus of the dipole moment. We approximated the direction of the dipole moment by that provided by the long-range contribution developed by Li and Hunt²⁹ using the parameters D_d and D_q computed by Bruch *et al.*³¹ We performed as many independent runs of 10^6 Monte Carlo samples as required to obtain a statistical uncertainty smaller than 60% of the propagated uncertainty from the potential and polarizability, which has been evaluated according to the method discussed in Sec. IV. In order to reach this target, we needed at least 30 independent runs at each temperature.

IV. PROPAGATION OF THE UNCERTAINTY

Apart from the statistical uncertainty of the Monte Carlo calculation, which can be in principle reduced at will given a sufficient supply of computational power, there are five other sources of uncertainty for $C_\varepsilon(T)$, which come from the propagation of the uncertainty in the potential-energy surfaces u_2 and u_3 , the polarizabilities α_2 and α_3 , and the dipole moment \mathbf{m}_3 . The standard way to estimate these uncertainties is to perform calculations of $C_\varepsilon(T)$ using perturbed quantities,^{40,41} (e.g., $u_3 + \delta u_3$ and $u_3 - \delta u_3$), obtaining perturbed values of the virial coefficients, say C_ε^+ and C_ε^- . Assuming that the uncertainty δu_3 is provided at coverage factor $k = 2$, the estimate of the standard uncertainty of the dielectric virial coefficient coming from the pair potential would be given by

$$\delta C_\varepsilon^{[u_3]} = \frac{1}{4} |C_\varepsilon^+ - C_\varepsilon^-|, \quad (21)$$

with analogous expressions for the two-body potential, the polarizabilities, and the dipole moment.

The main drawback of this approach is that the value of the propagated uncertainty δC_ε is not known in advance, and this requires performing long calculations of the perturbed virials so that the difference in Eq. (21) becomes smaller than the combined statistical uncertainties of C_ε^+ and C_ε^- . In a recent paper,⁴⁴ we put forward an alternative way to estimate $\delta C_\varepsilon(T)$, based on functional differentiation of the expressions leading to the virial coefficient with respect to potential, polarizability, and dipole-moment surfaces. We used the classical expressions for the virial coefficients, and we evaluated the resulting expressions using the fourth-order Feynman–Hibbs correction to the pair potential in order to take into account quantum effects.

In this paper, we extend this approach by taking directly the functional derivatives of the path-integral expressions, that is Eqs. (17)–(19). In this case, quantum effects are considered from the very start and we can safely proceed to evaluate propagated uncertainties down to very low temperatures, where a semiclassical approach would most likely fail. Additionally, we can include the uncertainty of exchange terms in a rigorous way. Since

the third dielectric virial coefficient is given by a sum of three terms, each of which depends on five different surfaces, there are 15 contributions to the overall uncertainty. We will discuss here only a few of them to point out the main features of the calculations. All of the contributions to the overall uncertainty are then summed in quadrature to produce the overall value of the propagated uncertainty. Explicit expressions for all 15 contributions to the uncertainty of C_ε are given in the Supplementary Material.

In calculating the variation of the third dielectric virial coefficient with respect to a quantity s with uncertainty δs ($s = u_2, u_3, \alpha_2, \alpha_3, \mathbf{m}_3$), which depends on some variables \mathbf{X} (\mathbf{X} is the radial distance in the case of u_2 and α_2 , or the three interatomic distances in the case of u_3, α_3 , and \mathbf{m}_3), one obtains for the propagated standard uncertainty the general formula

$$\delta C_\varepsilon^{[s]} = \frac{1}{2} \int \delta s \left| \frac{\delta C_\varepsilon}{\delta s} \right| d\mathbf{X}, \quad (22)$$

where the factor of 2 takes into account the fact that δs is an expanded uncertainty with coverage factor $k = 2$. Since the functional derivative $\delta C_\varepsilon/\delta s$ can in general have positive and negative values, we adopted the conservative choice of taking the absolute value of the integrand in Eq. (22).

Let us consider first how to propagate the uncertainty due to the isotropic part of the three-body polarizability $\alpha_3 = \text{tr}[\alpha_3]/3$ to the value of the Boltzmann component of the third dielectric virial coefficient. Inserting Eq. (17) in Eq. (22), one obtains, for the standard uncertainty,

$$\delta C_\varepsilon^{[\alpha_3]} = \frac{1}{2} \frac{2\pi}{9} \int \left| \left\langle \overline{\delta \alpha_3} e^{-\beta \overline{V_3}} \right\rangle \right| d\mathbf{r}_2 d\mathbf{r}_3, \quad (23)$$

and similarly, in the case of u_3 ,

$$\delta C_\varepsilon^{[u_3]} = \frac{1}{2} \frac{2\pi\beta}{9} \int \left| \left\langle \overline{\delta u_3} \overline{A_3} e^{-\beta \overline{V_3}} \right\rangle \right| d\mathbf{r}_2 d\mathbf{r}_3. \quad (24)$$

By performing the functional derivative of Eq. (17) with respect to the isotropic component of the pair polarizability and the pair potential, we obtain an expression for their contribution to the overall uncertainty

$$\delta C_\varepsilon^{[\alpha_2]} = \frac{1}{2} \frac{2\pi}{9} \int \left| \left\langle \sum_{i < j} \overline{\delta \alpha_{\text{iso}}}(\mathbf{r}_{ij}) \left(e^{-\beta \overline{V_3}} - e^{-\beta \overline{V_2}(\mathbf{r}_{ij})} \right) - 6 \left(e^{-\beta \overline{V_2}(\mathbf{r}_{12})} - 1 \right) \overline{\delta \alpha_{\text{iso}}}(\mathbf{r}_{13}) e^{-\beta \overline{V_2}(\mathbf{r}_{13})} \right\rangle \right| d\mathbf{r}_2 d\mathbf{r}_3 \quad (25)$$

$$\delta C_\varepsilon^{[u_2]} = \frac{1}{2} \frac{2\pi\beta}{9} \int \left| \left\langle \sum_{i < j} \overline{\delta u_2}(\mathbf{r}_{ij}) \left[\left(\frac{\beta |\overline{\mathbf{m}_3}|^2}{3} + \overline{A_3} \right) e^{-\beta \overline{V_3}} - \overline{\alpha_{\text{iso}}}(\mathbf{r}_{ij}) e^{-\beta \overline{V_2}(\mathbf{r}_{ij})} \right] - 6 \overline{\delta u_2}(\mathbf{r}_{12}) e^{-\beta \overline{V_2}(\mathbf{r}_{12})} \left(e^{-\beta \overline{V_2}(\mathbf{r}_{13})} (\overline{\alpha_{\text{iso}}}(\mathbf{r}_{12}) + \overline{\alpha_{\text{iso}}}(\mathbf{r}_{13})) - \overline{\alpha_{\text{iso}}}(\mathbf{r}_{12}) \right) \right\rangle \right| d\mathbf{r}_2 d\mathbf{r}_3, \quad (26)$$

and, finally, functional differentiation with respect to the

dipole moment gives

$$\delta C_\varepsilon^{[\mathbf{m}_3]} = \frac{1}{2} \frac{4\pi\beta}{27} \int \left| \left\langle \overline{\delta \mathbf{m}_3} \cdot \overline{\mathbf{m}_3} e^{-\beta \overline{V_3}} \right\rangle \right| d\mathbf{r}_2 d\mathbf{r}_3. \quad (27)$$

We notice that the last terms in Eqs. (25) and (26) explicitly involve the pairs 1–2 and 1–3. The integral, however, does not depend on the labels assigned to the particles and there are six possible ways to extract from three particles two pairs that have one label in common. In actual calculations, it is convenient to average over the symmetrization in all the possible pairs, which will conveniently remove the factor of 6 in front of the original expression. Furthermore, the values of the propagated uncertainties converge much faster than the dielectric virial calculations. We found that it was sufficient to use $P = \text{nint}(4 + 140 \text{ K}/T)$ with 200 000 Monte Carlo samples for both isotopes in order to have well-converged results.

V. RESULTS AND DISCUSSION

The results of our calculations are reported in Tables III and IV for the ^4He and ^3He isotopes, respectively. The two sets of data are mutually compatible, within expanded uncertainties, down to $T \sim 4$ K. Below this temperature, quantum exchange effects contribute significantly to the difference in C_ϵ between the two isotopes.

Table III also reports the values of all the contributions to C_ϵ that have been computed for this work: the value assuming only pair interactions (C_ϵ^{pair}), the contribution due to three-body properties ($C_\epsilon^{\text{diff-32}}$, which takes into account the three-body potential and polarizability), the dipole-moment contribution (C_ϵ^{dip} , coming from the terms proportional to \mathbf{m}_3 in Eqs. (17)–(19)), and the quantum statistical (exchange) contributions at low temperature, Eqs. (18) and (19). In general, the dipole-moment contribution is completely negligible at all the temperatures investigated here, as already noticed in our previous work¹⁶ where we used an approximate form for the dipole moment of the helium trimer due to Li and Hunt.²⁹ We note, however, that the values for the dipolar contribution that we obtain with the new dipole-moment surface are 3 to 20 times larger than the ones obtained with the surface of Ref. 29.

Quantum exchange contributions are found to be sizable (that is, comparable to the overall uncertainty of the calculation) below $T \sim 3$ K for both isotopes. When compared with our previous calculations,¹⁶ which used an approximate form of the three-body polarizability, the present values of C_ϵ are in reasonable agreement for most of the temperature range. As shown in Fig. 1, there is systematic upwards shift for $T > 300$ K, and the difference becomes larger than the uncertainty of the present calculation for $T > 1000$ K. Given the minor contribution from the dipole-moment surface, this good agreement means that the superposition approximation used in Ref. 16 for the non-additive three-body polarizability is quite good, at least in the case of helium. Since the behavior of virial coefficients at high temperatures is more sensitive to the short-range details of the potential and polarizability surfaces, we conclude that the superposition approximation

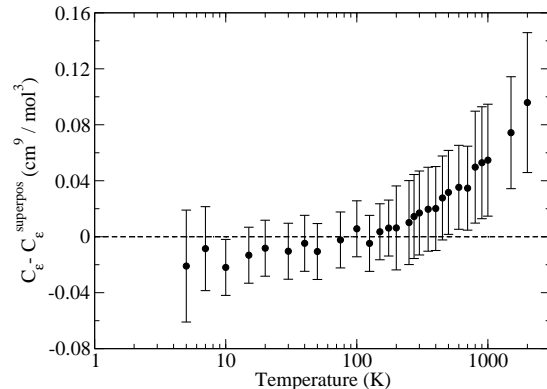


FIG. 1. The values of C_ϵ for ^4He computed in the present work using as a baseline the values computed using the superposition approximation for the three-body polarizability.¹⁶ Error bars correspond to expanded ($k = 2$) uncertainties.

is less accurate at short range than it is at long range. This conclusion agrees with a detailed analysis of the three-body polarizability surface performed in Ref. 17.

In our previous work, the use of the superposition approximation prevented a rigorous estimation of the overall uncertainty of the PIMC calculations, in contrast to the results presented here. As might be expected by comparing the present values of $U(C_\epsilon)$ to those of our previous work,¹⁶ the uncertainty budget of the third dielectric virial coefficient is dominated by the uncertainty of the three-body polarizability surface. In order to see that, a breakdown of various components of the overall uncertainty is reported in Fig. 2 in the case of the Boltzmann contribution $C_\epsilon^{\text{Boltz}}(T)$. For $T > 10$ K, the largest contribution by far to the overall propagated uncertainty comes from the uncertainty of the three-body polarizability, followed by the propagated uncertainty from the two-body polarizability. The latter becomes the dominant contribution for $T < 3.5$ K. Figure 2 shows that we managed to keep the statistical uncertainty of the calculations smaller than the largest contribution from the uncertainties propagated from potentials and polarizabilities. The contributions from the other three sources (the pair and three-body potential energy, as well as the dipole moment) are found to be negligible overall, being at least one order of magnitude smaller in the whole temperature range considered here. The individual uncertainty contributions presented in Fig. 2 are reported as Tables in the Supplementary Material.

Finally, let us compare our fully quantum results with a classical evaluation of the dielectric virial coefficient. As shown in Fig. 3, the classical approximation is quite good for $T > 200$ K. At lower temperatures, one can observe a systematic downward shift, which becomes larger than the uncertainty of the calculation for $T < 50$ K. For still lower temperatures, quantum effects are responsible for

TABLE III. Third dielectric virial coefficient C_ϵ for ^4He , its expanded uncertainty $U(C_\epsilon)$, together with the various contributions from the pair potential ($C_\epsilon^{:,2\text{-body}}$), the three-body potential and polarizability ($C_\epsilon^{:,diff-32}$), the dipole moment (C_ϵ^{dip}), and the exchange terms of Eqs. (18) and (19). $U(C_\epsilon)$ are expanded uncertainties at $k = 2$ and include the statistical uncertainty of the calculation as well as the propagated uncertainties from potentials, polarizabilities, and dipole moment.

Temperature (K)	C_ϵ ($\text{cm}^9 \text{mol}^{-3}$)	$U(C_\epsilon)$ (cm^9/mol^3)	$C_\epsilon^{:,2\text{-body}}$ (cm^9/mol^3)	$C_\epsilon^{:,diff-32}$ (cm^9/mol^3)	C_ϵ^{dip} ($10^{-5} \text{cm}^9/\text{mol}^3$)	$C_\epsilon^{\text{!}}$ (cm^9/mol^3)	C_ϵ^Δ (cm^9/mol^3)
1	-3.89	0.55	-1.832	-0.628	531.0	-0.5518	-0.8852
1.2	-2.26	0.35	-1.165	-0.465	433.6	-0.1541	-0.4840
1.4	-1.44	0.23	-0.744	-0.399	312.0	-0.0435	-0.2556
1.6	-1.07	0.18	-0.572	-0.348	250.4	-0.0153	-0.1392
1.8	-0.83	0.14	-0.448	-0.322	205.8	0.0128	-0.0786
2	-0.72	0.11	-0.388	-0.292	169.2	0.0090	-0.0485
2.1768	-0.62	0.10	-0.319	-0.288	146.3	0.0163	-0.0304
2.5	-0.51	0.08	-0.236	-0.268	114.7	0.0111	-0.0136
3	-0.39	0.06	-0.173	-0.224	85.6	0.0053	-0.0042
3.5	-0.34	0.05	-0.129	-0.217	68.1	0.0025	-0.0014
4	-0.31	0.05	-0.111	-0.198	56.3	0.0017	-0.0005
4.222	-0.29	0.04	-0.101	-0.193	51.7	0.0009	-0.0003
4.5	-0.28	0.04	-0.095	-0.188	47.2	0.0007	-0.0002
5	-0.27	0.04	-0.083	-0.186	40.8		
6	-0.24	0.03	-0.075	-0.168	32.3		
7	-0.23	0.03	-0.068	-0.166	26.7		
8	-0.22	0.03	-0.066	-0.157	22.9		
10	-0.23	0.02	-0.070	-0.156	18.1		
12	-0.22	0.02	-0.074	-0.148	15.3		
13.8031	-0.23	0.02	-0.080	-0.148	13.5		
15	-0.23	0.02	-0.083	-0.146	12.6		
17	-0.23	0.02	-0.090	-0.145	11.4		
20	-0.24	0.02	-0.100	-0.140	10.3		
24.5561	-0.25	0.02	-0.114	-0.134	9.1		
30	-0.27	0.02	-0.132	-0.134	8.3		
40	-0.29	0.02	-0.159	-0.132	7.5		
50	-0.32	0.02	-0.184	-0.134	7.2		
54.3584	-0.32	0.02	-0.193	-0.131	7.1		
60	-0.34	0.02	-0.205	-0.133	7.0		
75	-0.36	0.02	-0.233	-0.124	7.0		
83.8058	-0.37	0.02	-0.248	-0.125	7.1		
100	-0.39	0.02	-0.272	-0.123	7.2		
125	-0.43	0.02	-0.304	-0.124	7.6		
150	-0.45	0.02	-0.331	-0.119	8.0		
161.4	-0.46	0.02	-0.342	-0.119	8.2		
175	-0.47	0.02	-0.354	-0.114	8.4		
200	-0.49	0.03	-0.375	-0.114	8.8		
225	-0.50	0.03	-0.393	-0.111	9.2		
234.3156	-0.51	0.03	-0.399	-0.107	9.4		
250	-0.52	0.03	-0.409	-0.106	9.7		
273.16	-0.53	0.03	-0.423	-0.108	10.1		
300	-0.54	0.03	-0.438	-0.104	10.5		
302.9146	-0.54	0.03	-0.439	-0.103	10.6		
325	-0.55	0.03	-0.450	-0.099	10.9		
350	-0.56	0.03	-0.461	-0.098	11.4		
375	-0.57	0.03	-0.472	-0.098	11.8		
400	-0.58	0.03	-0.482	-0.098	12.2		
429.7485	-0.59	0.03	-0.492	-0.094	12.6		
450	-0.59	0.03	-0.499	-0.092	13.0		
500	-0.60	0.03	-0.515	-0.083	13.8		
600	-0.62	0.03	-0.541	-0.081	15.3		
700	-0.64	0.03	-0.562	-0.077	16.8		
800	-0.64	0.04	-0.579	-0.065	18.2		
900	-0.65	0.04	-0.593	-0.054	19.6		
1000	-0.66	0.04	-0.605	-0.055	21.0		
1500	-0.67	0.04	-0.644	-0.027	27.6		
2000	-0.66	0.05	-0.662	0.002	33.8		
2500	-0.65	0.05	-0.670	0.021	39.7		
3000	-0.62	0.06	-0.672	0.053	45.5		

TABLE IV. Third dielectric virial coefficient C_ε for ^3He , its expanded uncertainty $U(C_\varepsilon)$, together with the various contributions from the pair potential ($C_\varepsilon^{:,2\text{-body}}$), the three-body potential and polarizability ($C_\varepsilon^{:,diff-32}$), the dipole moment ($C_\varepsilon^{\text{dip}}$), and the exchange terms of Eqs. (18) and (19). $U(C_\varepsilon)$ are expanded uncertainties at $k=2$ and include the statistical uncertainty of the calculation as well as the propagated uncertainties from potentials, polarizabilities, and dipole moment.

Temperature (K)	C_ε (cm^9/mol^3)	$U(C_\varepsilon)$ (cm^9/mol^3)	$C_\varepsilon^{:,2\text{-body}}$ (cm^9/mol^3)	$C_\varepsilon^{:,diff-32}$ (cm^9/mol^3)	$C_\varepsilon^{\text{dip}}$ ($10^{-5} \text{cm}^9/\text{mol}^3$)	C_ε^{I} (cm^9/mol^3)	C_ε^{Δ} (cm^9/mol^3)
1	-0.57	0.28	-0.268	-0.249	227.0	0.05425	-0.10561
1.2	-0.50	0.19	-0.217	-0.236	181.4	0.01796	-0.06916
1.4	-0.45	0.14	-0.182	-0.226	152.2	0.00412	-0.04802
1.6	-0.42	0.10	-0.157	-0.228	128.1	-0.00651	-0.03131
1.8	-0.39	0.09	-0.140	-0.223	112.4	-0.00785	-0.02180
2	-0.37	0.08	-0.121	-0.225	96.6	-0.01053	-0.01505
2.2	-0.33	0.07	-0.113	-0.198	85.7	-0.00890	-0.01035
2.4	-0.33	0.06	-0.102	-0.209	77.1	-0.01071	-0.00730
2.5	-0.31	0.06	-0.097	-0.199	72.6	-0.01014	-0.00611
2.6	-0.31	0.06	-0.095	-0.209	69.7	-0.00656	-0.00518
2.8	-0.29	0.05	-0.093	-0.191	64.2	-0.00474	-0.00372
3	-0.29	0.05	-0.088	-0.197	58.8	-0.00557	-0.00264
3.2	-0.27	0.05	-0.085	-0.184	54.3	-0.00469	-0.00190
3.4	-0.27	0.04	-0.081	-0.183	50.7	-0.00289	-0.00135
3.5	-0.27	0.04	-0.081	-0.186	49.4	-0.00305	-0.00115
3.6	-0.26	0.04	-0.080	-0.173	47.6	-0.00302	-0.00099
4	-0.26	0.04	-0.076	-0.181	42.6	-0.00233	-0.00052
4.5	-0.26	0.03	-0.073	-0.181	37.4	-0.00119	-0.00025
5	-0.24	0.03	-0.072	-0.167	33.3	-0.00069	-0.00012
6	-0.23	0.03	-0.071	-0.163	27.7	-0.00026	-0.00003
7	-0.24	0.02	-0.070	-0.165	23.8		
8	-0.23	0.02	-0.073	-0.157	21.0		
10	-0.23	0.02	-0.079	-0.152	17.3		
12	-0.24	0.02	-0.084	-0.152	14.9		
15	-0.24	0.02	-0.094	-0.147	12.7		
20	-0.25	0.02	-0.110	-0.145	10.6		
25	-0.26	0.02	-0.126	-0.136	9.4		
30	-0.28	0.02	-0.140	-0.137	8.7		
40	-0.30	0.02	-0.167	-0.137	7.9		
50	-0.32	0.02	-0.190	-0.135	7.6		
60	-0.35	0.02	-0.211	-0.136	7.4		
75	-0.36	0.02	-0.238	-0.127	7.4		
80	-0.37	0.02	-0.246	-0.125	7.4		
100	-0.40	0.02	-0.276	-0.125	7.6		
125	-0.43	0.02	-0.307	-0.122	7.9		
150	-0.45	0.02	-0.334	-0.118	8.2		
175	-0.47	0.02	-0.357	-0.115	8.6		
200	-0.49	0.03	-0.377	-0.112	9.0		
225	-0.50	0.03	-0.395	-0.110	9.5		
250	-0.52	0.03	-0.411	-0.110	9.9		
273.16	-0.53	0.03	-0.425	-0.106	10.3		
300	-0.54	0.03	-0.439	-0.102	10.7		
350	-0.56	0.03	-0.463	-0.101	11.5		
400	-0.58	0.03	-0.483	-0.098	12.3		
450	-0.60	0.03	-0.501	-0.097	13.1		
500	-0.61	0.03	-0.516	-0.096	13.9		
600	-0.62	0.03	-0.542	-0.083	15.4		
700	-0.64	0.04	-0.563	-0.074	16.9		
750	-0.64	0.04	-0.572	-0.071	17.6		
800	-0.64	0.04	-0.580	-0.063	18.3		
900	-0.65	0.04	-0.594	-0.057	19.8		
1000	-0.66	0.04	-0.606	-0.050	21.1		
1500	-0.67	0.04	-0.644	-0.026	27.7		
2000	-0.66	0.05	-0.662	0.001	33.9		
2500	-0.65	0.05	-0.670	0.019	39.8		
3000	-0.63	0.06	-0.672	0.045	45.5		

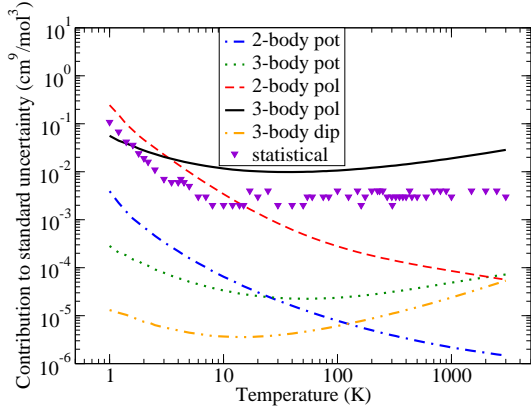


FIG. 2. The various contributions to the standard uncertainty of C_ϵ in the case of ^4He . Solid line: the three-body polarizability. Dashed line: the pair polarizability. Dotted line: the three-body potential. Dot-dashed line: the pair potential. Dot-dot-dashed line: the three-body dipole. Triangles: statistical uncertainty from PIMC calculations.

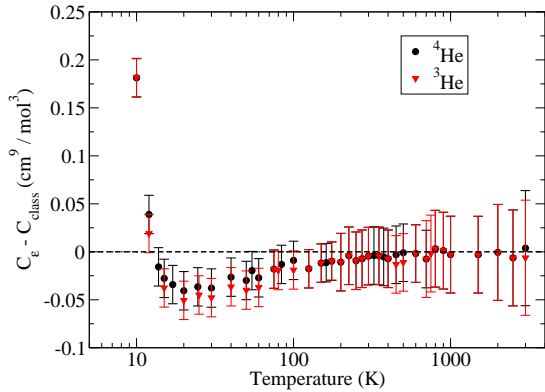


FIG. 3. The difference between the fully quantum calculation of C_ϵ and the classical approximation. Circles: ^4He , triangles: ^3He . Error bars correspond to expanded ($k = 2$) uncertainties.

a significant upwards shift of the PIMC calculations. As already noted when comparing the quantum results for the two isotopes, the ^4He and ^3He results agree within their mutual uncertainties at all the temperatures shown in Fig. 3.

A. Correlation for C_ϵ

Values of C_ϵ at temperatures not reported in Tables III and IV can be obtained in principle by interpolating the tabulated values. However, given the relatively large error bars, this procedure could produce spurious values.

TABLE V. Parameters for the correlations (28) and (29) in the case of ^4He and ^3He . The a_i and A_i are given in cm^9/mol^3 while the b_i and c_i are dimensionless.

Parameter	Value for ^4He	Value for ^3He
a_1	-2288.7466	-363.45319
a_2	5191.1178	823.97628
a_3	-4363.9948	-902.48768
a_4	1461.3638	692.44074
a_5	-1.83960×10^{-3}	-250.75032
b_1	9/20	9/20
b_2	8/17	1/2
b_3	1/2	10/17
b_4	10/19	2/3
b_5	47/20	5/7
A_0	0.025	0.02
A_1	0.56	0.25
c_1	2.5	2
A_2	1.3×10^{-5}	2×10^{-4}
c_2	1	2/3

Here we provide parameters for a smooth correlation for both C_ϵ and its $k = 2$ uncertainty $U(C_\epsilon)$. For the former, we note that the target accuracy of a fitting function should be given by only the statistical uncertainty of the C_ϵ calculation, since the other contributions to the uncertainty are systematic. We have fitted the results to the expansion

$$C_\epsilon(T) = \sum_{k=1}^6 \frac{a_k}{(T/T_0)^{b_k}}, \quad (28)$$

with $T_0 = 30$ K, whereas for the expanded uncertainty we have used the representation

$$U(C_\epsilon)(T) = A_0 + \frac{A_1}{(T/1 \text{ K})^{c_1}} + A_2(T/1 \text{ K})^{c_2}, \quad (29)$$

whose parameters are reported in Table V for both ^4He and ^3He . All the values of $C_\epsilon(T)$ computed using the correlation at the 59 temperatures considered in this work (56 for ^3He) fall within the expanded statistical uncertainty of the PIMC calculation.

VI. COMPARISON WITH EXPERIMENT

As a second-order correction, C_ϵ is difficult to obtain from experiment. A few measurements with large uncertainties exist for ^4He ; we are not aware of any experimental data for ^3He . Figure 4 shows the scattered data available for the third dielectric virial coefficient of ^4He near room temperature. Our calculated results are the open circles; their error bars, corresponding to expanded ($k = 2$) uncertainties, are similar to the size of the symbols. For most of the experimental sources, the error bars are as given by the authors but the statistical meaning of their error interval was not stated.

The dielectric-constant gas thermometry measurements of Gaiser and Fellmuth⁴⁸ at 273.16 K did have

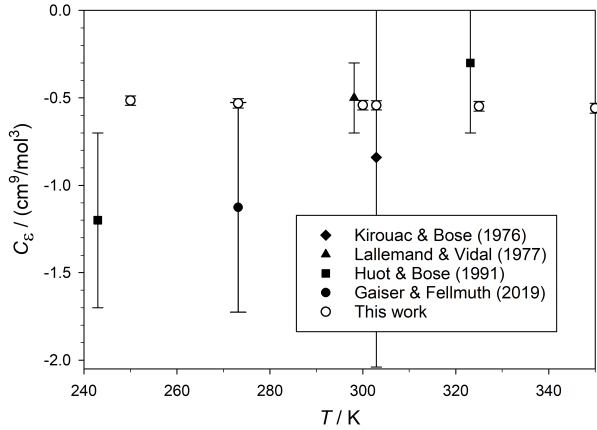


FIG. 4. Comparison of calculated values of the third dielectric virial coefficient $C_\epsilon(T)$ for ^4He with those derived from experiment^{45–48} near room temperature. Error bars for this work represent expanded ($k = 2$) uncertainties.

a complete uncertainty budget; the corresponding point in Fig. 4 is plotted with $k = 2$ error bars. Gaiser and Fellmuth reported a quantity that is a combination of the second and third density virial coefficients and the second and third dielectric virial coefficients. Since C_ϵ is the least accurately known of these four quantities, it can be derived with an uncertainty essentially the same as that for the reported quantity. To derive C_ϵ , we used state-of-the-art values for the second¹³ and third⁴⁹ density virial coefficients and for the second dielectric virial coefficient,¹⁶ resulting in a value of $-1.126 \text{ cm}^9 \text{ mol}^{-3}$ for C_ϵ with a $k = 2$ uncertainty of $0.60 \text{ cm}^9 \text{ mol}^{-3}$. This is slightly less negative than the value we derived and plotted in Ref. 16 due to our use of an improved value for the third density virial coefficient.⁴⁹ This datum is consistent with our calculated result within its expanded uncertainty, but barely so.

Figure 5 shows the results at lower temperatures; the $k = 2$ error bars for our calculated results are smaller than the size of the symbols above approximately 3 K. Our result is in modest disagreement with the point from Huot and Bose⁴⁷ near 77 K, but with much smaller uncertainty. At the lowest temperatures, the points from White and Gugan⁵⁰ have even larger uncertainties; they are at best in rough qualitative agreement with our calculations.

We examine the low-temperature data of White and Gugan⁵⁰ more closely in Fig. 6; on this scale the error bars for our calculations are only visible below approximately 2 K. Figure 6 makes clear that, if one were to infer a temperature dependence of C_ϵ from the values reported by White and Gugan, the slope would have the wrong sign. We note that even White and Gugan did not take their temperature dependence too seriously; they ultimately recommended a single value of C_ϵ corresponding to $(-2.6 \pm 2.1) \text{ cm}^9 \text{ mol}^{-3}$ to represent their entire experimental range from 3 K to 18 K. This value is inconsis-

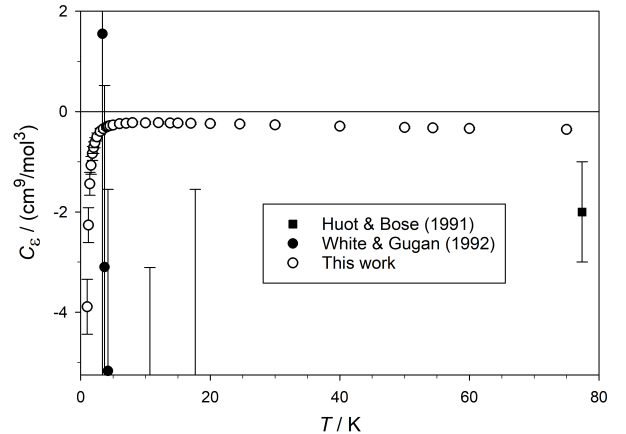


FIG. 5. Comparison of calculated values of the third dielectric virial coefficient $C_\epsilon(T)$ for ^4He with those derived from experiment^{47,50} at low temperatures. The two highest temperature points from Ref. 50 are below the bottom of the plot; only the tops of their error bars are visible.

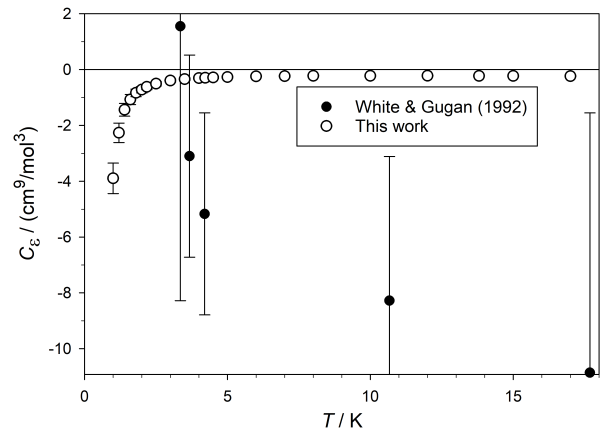


FIG. 6. Comparison of calculated values of the third dielectric virial coefficient $C_\epsilon(T)$ for ^4He with those from White and Gugan⁵⁰ below 18 K.

tent with our results, but our points would be contained in their large uncertainty range if their uncertainty estimate was larger by an additional 15%. In Ref. 15, it was noted that the agreement between highly accurate, rigorously calculated values of B_ϵ and those reported by White and Gugan was strikingly good, especially considering the challenging nature of their experiments at these low temperatures. It seems that this good agreement was limited to $B_\epsilon(T)$, and that White and Gugan did not derive meaningful experimental values of C_ϵ .

VII. CONCLUSIONS

To support new developments in thermodynamic temperature and pressure metrology, this work presents the first complete *ab initio* calculation of the third dielectric virial coefficient, C_ϵ , of helium. All physical effects are considered (including quantum statistical effects that become important at low temperatures), and state-of-the-art first-principles surfaces are used for the pair and three-body potentials, the pair and three-body polarizabilities, and the three-body dipole moment. Uncertainties from each of the surfaces, and from the path-integral Monte Carlo calculations used to compute C_ϵ with rigorous consideration of quantum effects, are combined to yield a complete estimate for the uncertainty of $C_\epsilon(T)$.

Since no previous *ab initio* surface existed for the dipole moment of an assembly of three helium atoms, a dipole-moment surface was developed in this work. The *ab initio* calculations of the dipole moment accounted for electron correlation with the CC3 method and employed doubly augmented QZ basis sets that had been developed previously.²⁶ Some calculations with full correlation of all electrons and some with larger basis sets were performed to assess uncertainty due to incompleteness of the calculations. The results for the magnitude of the three-body dipole moment were fitted to a function that was constrained to obey boundary conditions known from theory. At all temperatures considered, the contribution of the three-body dipole term to C_ϵ is roughly two orders of magnitude smaller than the expanded uncertainty in C_ϵ , making it effectively negligible in this context. We could not have drawn that conclusion with certainty without the present effort to calculate the contribution rigorously.

Our results for C_ϵ are generally consistent with previous work¹⁶ that employed approximations for the three-body polarizability and dipole-moment surfaces and that used a now-obsolete surface for the three-body potential energy. At temperatures above 300 K, our new values of C_ϵ are systematically higher (less negative), suggesting inaccuracy in the short-range behavior of the superposition approximation for the three-body polarizability that was used in Ref. 16.

At most temperatures, the uncertainty budget of C_ϵ is dominated by the uncertainty of the three-body polarizability surface (see Fig. 2). Since that surface was recently developed with state-of-the-art methods,¹⁷ improvement of that contribution in the near future seems unlikely. Below about 10 K, the nonadditive pair polarizability also makes a significant contribution to the uncertainty budget, becoming the largest component below roughly 3.5 K. The pair polarizability function is now more than ten years old,¹⁴ so improving it may be a worthwhile effort, especially if it is planned to use gas-based dielectric or refractive measurements for temperature metrology below 10 K.

Our results also enable better refractivity-based metrology, the working equations of which employ a virial

expansion similar to Eq. (1) but with refractivity virial coefficients B_R and C_R . At microwave frequencies, C_R is effectively identical to the C_ϵ derived here. At optical and near-infrared frequencies, a dispersion correction to C_ϵ is needed for rigorous calculation of C_R . To our knowledge, the information needed to make this correction has not been derived. However, the relatively small differences (less than 10% and often less than 5%) between B_ϵ and B_R for helium at optical frequencies¹⁵ suggests that, in the absence of other information, $C_\epsilon(T)$ can provide a reasonable approximation to $C_R(T)$ in this regime.

VIII. SUPPLEMENTARY MATERIAL

- Formulae for propagating the uncertainty of potentials, polarizabilities, and dipole moment to the various components of C_ϵ .
- Table of the propagated uncertainties for ^4He reported in Fig. 2.
- Plot illustrating the accuracy of the fit of the three-body dipole moment.
- Raw *ab initio* results CC3[d4Z] for all 734 configurations considered in this work, and CC3[a3Z] and FCI[a3Z] results for configurations given in Table II.
- Optimized parameters of the fitting function (5).
- FORTRAN program to compute the squared modulus of the dipole moment of a system of three He atoms.

ACKNOWLEDGMENTS

B.J., G.G., and J.L. acknowledge support from *QuantumPascal* project 18SIB04, which has received funding from the EMPIR programme co-financed by the Participating States and from the European Union's Horizon 2020 research and innovation programme. G.G. ac-

knowledges CINECA (Award No. IscraC-THIDIVI) under the ISCRA initiative for the availability of high-performance computing resources and support. We gratefully acknowledge Poland's high-performance Infrastructure PLGrid (HPC Centers: ACK Cyfronet AGH, PCSS, CI TASK, WCSS) for providing computer facilities and support within computational grants PLG/2023/016599 and PLG/2024/017370.

AUTHOR DECLARATIONS

Conflict of Interest

The authors have no conflicts to disclose.

DATA AVAILABILITY

The data that support the findings of this study are available within the article and its Supplementary Material.

IX. SUPPLEMENTARY MATERIAL

A. Formulae for the propagated uncertainties of C_ϵ

1. Boltzmann component, \therefore

These equations are already reported in the main text and are reproduced here for completeness

$$\delta C_\epsilon^{\therefore[u_2]} = \frac{\pi\beta}{9} \int \left| \left\langle \sum_{i<j} \overline{\delta u_2}(\mathbf{r}_{ij}) \left[\left(\frac{\beta |\overline{\mathbf{m}_3^{\therefore}}|^2}{3} + \overline{A_3^{\therefore}} \right) e^{-\beta \overline{V_3^{\therecirc}}} - \overline{\alpha_{\text{iso}}}(\mathbf{r}_{ij}) e^{-\beta \overline{V_2^{\therecirc}}(\mathbf{r}_{ij})} \right] - 6 \overline{\delta u_2}(\mathbf{r}_{12}) e^{-\beta \overline{V_2^{\therecirc}}(\mathbf{r}_{12})} \left(e^{-\beta \overline{V_2^{\therecirc}}(\mathbf{r}_{13})} (\overline{\alpha_{\text{iso}}}(\mathbf{r}_{12}) + \overline{\alpha_{\text{iso}}}(\mathbf{r}_{13})) - \overline{\alpha_{\text{iso}}}(\mathbf{r}_{12}) \right) \right| \right\rangle \right| \mathbf{d}\mathbf{r}_2 \mathbf{d}\mathbf{r}_3, \quad (30)$$

$$\delta C_\epsilon^{\therefore[u_3]} = \frac{\pi\beta}{9} \int \left| \left\langle \overline{\delta u_3} \left(\frac{\beta |\overline{\mathbf{m}_3^{\therecirc}}|^2}{3} + \overline{A_3^{\therecirc}} \right) e^{-\beta \overline{V_3^{\therecirc}}} \right| \right\rangle \right| \mathbf{d}\mathbf{r}_2 \mathbf{d}\mathbf{r}_3 \quad (31)$$

$$\delta C_\epsilon^{\therecirc[\alpha_2]} = \frac{\pi}{9} \int \left| \left\langle \sum_{i<j} \overline{\delta \alpha_{\text{iso}}}(\mathbf{r}_{ij}) \left(e^{-\beta \overline{V_3^{\therecirc}}} - e^{-\beta \overline{V_2^{\therecirc}}(\mathbf{r}_{ij})} \right) - 6 \left(e^{-\beta \overline{V_2^{\therecirc}}(\mathbf{r}_{12})} - 1 \right) \overline{\delta \alpha_{\text{iso}}}(\mathbf{r}_{13}) e^{-\beta \overline{V_2^{\therecirc}}(\mathbf{r}_{13})} \right| \right\rangle \right| \mathbf{d}\mathbf{r}_2 \mathbf{d}\mathbf{r}_3 \quad (32)$$

$$\delta C_\epsilon^{\therecirc[\alpha_3]} = \frac{\pi}{9} \int \left| \left\langle \overline{\delta \alpha_3} e^{-\beta \overline{V_3^{\therecirc}}} \right| \right\rangle \right| \mathbf{d}\mathbf{r}_2 \mathbf{d}\mathbf{r}_3 \quad (33)$$

$$\delta C_\epsilon^{\therecirc[\mathbf{m}_3]} = \frac{2\pi\beta}{27} \int \left| \left\langle \overline{\delta \mathbf{m}_3^{\therecirc}} \cdot \overline{\mathbf{m}_3^{\therecirc}} e^{-\beta \overline{V_3^{\therecirc}}} \right| \right\rangle \right| \mathbf{d}\mathbf{r}_2 \mathbf{d}\mathbf{r}_3 \quad (34)$$

2. Odd component, \cdot

$$\begin{aligned} \delta C_\varepsilon^{\cdot[u_2]} &= \frac{(-1)^{2I}}{2I+1} \frac{\pi\beta\Lambda^3}{3 \cdot 2^{3/2}} \int \left| \left\langle \sum_{i<j} \overline{\delta u_2^{\cdot}} \left(\frac{\beta|\mathbf{m}_3^{\cdot}|^2}{3} + \overline{A_3^{\cdot}} \right) e^{-\beta V_3^{\cdot}} - \overline{\delta u_2^{\cdot} \alpha_{\text{iso}}^{\cdot}} e^{-\beta V_2^{\cdot}} \right\rangle \right. \\ &\quad - 2 \left\langle \overline{\delta u_2^{\cdot}} e^{-\beta V_2^{\cdot}} \right\rangle \left\langle \overline{\alpha_{\text{iso}}^{\cdot}} e^{-\beta V_2^{\cdot}} \right\rangle - 2 \left\langle e^{-\beta V_2^{\cdot}} \right\rangle \left\langle \overline{\delta u_2^{\cdot} \alpha_{\text{iso}}^{\cdot}} e^{-\beta V_2^{\cdot}} \right\rangle \\ &\quad \left. - 2 \left\langle \overline{\delta u_2^{\cdot} \alpha_{\text{iso}}^{\cdot}} e^{-\beta V_2^{\cdot}} \right\rangle \left\langle e^{-\beta V_2^{\cdot}} - 1 \right\rangle - 2 \left\langle \overline{\alpha_{\text{iso}}^{\cdot}} e^{-\beta V_2^{\cdot}} \right\rangle \left\langle \overline{\delta u_2^{\cdot}} e^{-\beta V_2^{\cdot}} \right\rangle \right| \mathbf{d}\mathbf{r} \end{aligned} \quad (35)$$

$$\delta C_\varepsilon^{\cdot[u_3]} = \frac{(-1)^{2I}}{2I+1} \frac{\pi\beta\Lambda^3}{3 \cdot 2^{3/2}} \int \left| \left\langle \overline{\delta u_3^{\cdot}} \left(\frac{\beta|\mathbf{m}_3^{\cdot}|^2}{3} + \overline{A_3^{\cdot}} \right) e^{-\beta V_3^{\cdot}} \right\rangle \right| \mathbf{d}\mathbf{r} \quad (36)$$

$$\begin{aligned} \delta C_\varepsilon^{\cdot[\alpha_2]} &= \frac{(-1)^{2I}}{2I+1} \frac{\pi\Lambda^3}{3 \cdot 2^{3/2}} \int \left| \left\langle \sum_{i<j} \overline{\delta \alpha_{\text{iso}}^{\cdot}}(\mathbf{r}_{ij}) e^{-\beta V_3^{\cdot}} - \overline{\delta \alpha_{\text{iso}}^{\cdot}} e^{\beta V_2^{\cdot}} \right\rangle \right. \\ &\quad \left. - 2 \left\langle \overline{\delta \alpha_{\text{iso}}^{\cdot}}(\mathbf{r}) e^{-\beta V_2^{\cdot}} \right\rangle \left\langle e^{-\beta V_2^{\cdot}} \right\rangle - 2 \left\langle \overline{\delta \alpha_{\text{iso}}^{\cdot}} e^{-\beta V_2^{\cdot}} \right\rangle \left\langle e^{-\beta V_2^{\cdot}}(\mathbf{r}) - 1 \right\rangle \right| \mathbf{d}\mathbf{r} \end{aligned} \quad (37)$$

$$\delta C_\varepsilon^{\cdot[\alpha_3]} = \frac{(-1)^{2I}}{2I+1} \frac{\pi\Lambda^3}{3 \cdot 2^{3/2}} \int \left| \left\langle \overline{\delta \alpha_3^{\cdot}} e^{-\beta V_3^{\cdot}} \right\rangle \right| \mathbf{d}\mathbf{r} \quad (38)$$

$$\delta C_\varepsilon^{\cdot[\mathbf{m}_3]} = \frac{(-1)^{2I}}{2I+1} \frac{\pi\beta\Lambda^3}{9 \cdot 2^{3/2}} \int \left| \left\langle \overline{\delta \mathbf{m}_3^{\cdot}} \cdot \overline{\mathbf{m}_3^{\cdot}} e^{-\beta V_3^{\cdot}} \right\rangle \right| \mathbf{d}\mathbf{r} \quad (39)$$

3. Even component, Δ

$$\begin{aligned} \delta C_\varepsilon^{\Delta[u_2]} &= \frac{1}{(2I+1)^2} \frac{2\pi\beta\Lambda^3}{3} \left| \left\langle \frac{1}{3^{5/2}} \sum_{i<j} \overline{\delta u_2^{\Delta}}(\mathbf{r}_{ij}) \left(\frac{\beta|\mathbf{m}_3^{\Delta}|^2}{3} + \overline{A_3^{\Delta}} \right) e^{-\beta V_3^{\Delta}} \right\rangle \right. \\ &\quad \left. - \frac{1}{4} \left\langle \overline{\delta V_2^{\Delta}} e^{-\beta V_2^{\Delta}} \right\rangle \left\langle \overline{\alpha_{\text{iso}}^{\Delta}} e^{-\beta V_2^{\Delta}} \right\rangle - \frac{1}{4} \left\langle e^{-\beta V_2^{\Delta}} \right\rangle \left\langle \overline{\delta V_2^{\Delta} \alpha_{\text{iso}}^{\Delta}} e^{-\beta V_2^{\Delta}} \right\rangle \right| \end{aligned} \quad (40)$$

$$\delta C_\varepsilon^{\Delta[u_3]} = \frac{1}{(2I+1)^2} \frac{2\pi\beta\Lambda^3}{3^{7/2}} \left| \left\langle \overline{\delta u_3^{\Delta}} \left(\frac{\beta|\mathbf{m}_3^{\Delta}|^2}{3} + \overline{A_3^{\Delta}} \right) e^{-\beta V_3^{\Delta}} \right\rangle \right| \quad (41)$$

$$\delta C_\varepsilon^{\Delta[\alpha_2]} = \frac{1}{(2I+1)^2} \frac{2\pi\Lambda^6}{3} \left| \left\langle \frac{1}{3^{5/2}} \sum_{i<j} \overline{\delta \alpha_2^{\Delta}}(\mathbf{r}_{ij}) e^{-\beta V_3^{\Delta}} \right\rangle - \frac{1}{4} \left\langle \overline{\delta \alpha_{\text{iso}}^{\Delta}} e^{-\beta V_2^{\Delta}} \right\rangle \left\langle e^{-\beta V_2^{\Delta}} \right\rangle \right| \quad (42)$$

$$\delta C_\varepsilon^{\Delta[\alpha_3]} = \frac{1}{(2I+1)^2} \frac{2\pi\Lambda^6}{3^{7/2}} \left| \left\langle \overline{\delta \alpha_3^{\Delta}} e^{-\beta V_3^{\Delta}} \right\rangle \right| \quad (43)$$

$$\delta C_\varepsilon^{\Delta[\mathbf{m}_3]} = \frac{1}{(2I+1)^2} \frac{2\pi\beta\Lambda^6}{3^{9/2}} \left| \left\langle \overline{\delta \mathbf{m}_3^{\Delta}} \cdot \overline{\mathbf{m}_3^{\Delta}} e^{-\beta V_3^{\Delta}} \right\rangle \right| \quad (44)$$

B. Contributions to the uncertainty of C_ε^{\cdot}

Table VI shows the data plotted in Figure 2 of the main paper.

TABLE VI. Values of the components of the standard uncertainty of the Boltzmann part of C_ϵ for ^4He .

Temperature (K)	$u(V_2)$ (cm^9/mol^3)	$u(V_3)$ (cm^9/mol^3)	$u(\alpha_2)$ (cm^9/mol^3)	$u(\alpha_3)$ (cm^9/mol^3)	$u(\mathbf{m}_3)$ (cm^9/mol^3)
1	3.94E-03	2.84E-04	2.45E-01	5.61E-02	1.31E-05
1.4	1.48E-03	1.81E-04	9.89E-02	3.89E-02	1.04E-05
1.8	8.50E-04	1.39E-04	5.67E-02	3.05E-02	8.17E-06
2	6.91E-04	1.13E-04	4.65E-02	2.78E-02	7.46E-06
2.5	4.61E-04	9.21E-05	3.14E-02	2.34E-02	6.35E-06
3	3.40E-04	7.83E-05	2.28E-02	2.04E-02	5.72E-06
3.5	2.69E-04	6.77E-05	1.76E-02	1.86E-02	5.29E-06
4	2.21E-04	6.05E-05	1.41E-02	1.72E-02	4.93E-06
4.5	1.85E-04	5.70E-05	1.16E-02	1.61E-02	4.66E-06
5	1.58E-04	5.08E-05	9.86E-03	1.53E-02	4.43E-06
10	6.49E-05	3.35E-05	3.43E-03	1.17E-02	3.68E-06
15	4.11E-05	2.81E-05	1.96E-03	1.06E-02	3.58E-06
20	3.07E-05	2.57E-05	1.36E-03	1.02E-02	3.67E-06
30	2.07E-05	2.35E-05	8.43E-04	9.89E-03	3.94E-06
50	1.33E-05	2.26E-05	4.98E-04	9.94E-03	4.58E-06
75	9.69E-06	2.30E-05	3.48E-04	1.03E-02	5.35E-06
100	7.86E-06	2.36E-05	2.79E-04	1.06E-02	6.10E-06
150	5.96E-06	2.56E-05	2.12E-04	1.14E-02	7.46E-06
200	4.98E-06	2.75E-05	1.79E-04	1.21E-02	8.71E-06
250	4.33E-06	2.94E-05	1.58E-04	1.27E-02	9.89E-06
273.16	4.12E-06	3.03E-05	1.52E-04	1.30E-02	1.04E-05
300	3.92E-06	3.12E-05	1.45E-04	1.33E-02	1.10E-05
400	3.37E-06	3.45E-05	1.26E-04	1.43E-02	1.31E-05
500	3.00E-06	3.73E-05	1.14E-04	1.53E-02	1.50E-05
600	2.74E-06	4.00E-05	1.05E-04	1.61E-02	1.69E-05
800	2.41E-06	4.48E-05	9.37E-05	1.77E-02	2.05E-05
900	2.29E-06	4.69E-05	8.94E-05	1.83E-02	2.22E-05
1000	2.18E-06	4.88E-05	8.56E-05	1.90E-02	2.39E-05
2000	1.69E-06	6.32E-05	6.56E-05	2.44E-02	3.95E-05
3000	1.48E-06	7.23E-05	5.62E-05	2.86E-02	5.37E-05

C. Fitting accuracy of the three-body dipole moment

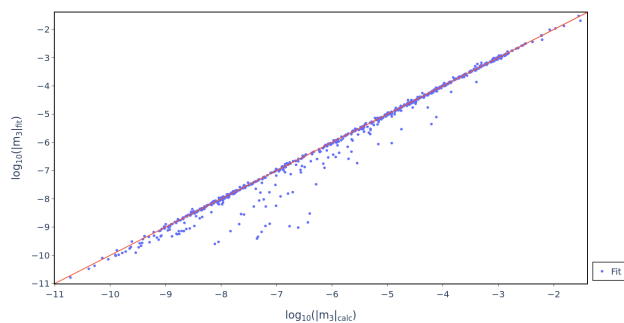


FIG. 7. Comparison of the fitted ($|\mathbf{m}_3|_{\text{fit}}$) and *ab initio* calculated ($|\mathbf{m}_3|_{\text{cal}}$) lengths of the three-body dipole moments for helium for all 734 geometries considered in the work. A logarithmic scale (base 10) is used on both axes of the plot. A linear function $y = x$ is added in red for comparison.

- ¹C. Gaiser, T. Zandt, and B. Fellmuth, “Dielectric-constant gas thermometry,” *Metrologia* **52**, S217–S226 (2015).
- ²C. Gaiser, B. Fellmuth, and N. Haft, “Primary thermometry from 2.5 K to 140 K applying dielectric-constant gas thermometry,” *Metrologia* **54**, 141–147 (2017).
- ³C. Gaiser, B. Fellmuth, and N. Haft, “Thermodynamic-temperature data from 30 K to 200 K,” *Metrologia* **57**, 055003 (2020).
- ⁴P. M. C. Rourke, C. Gaiser, B. Gao, D. Madonna Ripa, M. R. Moldover, L. Pitre, and R. J. Underwood, “Refractive-index gas thermometry,” *Metrologia* **56**, 032001 (2019).
- ⁵B. Gao, H. Zhang, D. Han, C. Pan, H. Chen, Y. Song, W. Liu, J. Hu, X. Kong, F. Sparasci, M. Plimmer, E. Luo, and L. Pitre, “Measurement of thermodynamic temperature between 5 K and 24.5 K with single-pressure refractive-index gas thermometry,” *Metrologia* **57**, 065006 (2020).
- ⁶D. Madonna Ripa, D. Imbraguglio, C. Gaiser, P. P. M. Steur, D. Giraudi, M. Fogliati, M. Bertinetti, G. Lopardo, R. Dematteis, and R. M. Gavioso, “Refractive index gas thermometry between 13.8 K and 161.4 K,” *Metrologia* **58**, 025008 (2021).
- ⁷P. M. C. Rourke, “Perspectives on the refractive-index gas metrology data landscape,” *J. Phys. Chem. Ref. Data* **50**, 033104 (2021).
- ⁸M. R. Moldover, R. M. Gavioso, J. B. Mehl, L. Pitre, M. de Podesta, and J. T. Zhang, “Acoustic gas thermometry,” *Metrologia* **51**, R1–R19 (2014).
- ⁹C. Gaiser, B. Fellmuth, and W. Sabuga, “Primary gas-pressure standard from electrical measurements and thermophysical *ab initio* calculations,” *Nature Phys.* **16**, 177–180 (2020).
- ¹⁰C. Gaiser, B. Fellmuth, and W. Sabuga, “Primary gas pressure standard passes next stress test,” *Ann. Physik* **534**, 2200336 (2022).
- ¹¹G. Garberoglio, C. Gaiser, R. M. Gavioso, A. H. Harvey, R. Hellmann, B. Jeziorski, K. Meier, M. R. Moldover, L. Pitre, K. Szalewicz, and R. Underwood, “*Ab Initio* calculation of fluid properties for precision metrology,” *J. Phys. Chem. Ref. Data* **52**, 031502 (2023).
- ¹²M. Puchalski, K. Szalewicz, M. Lesiuk, and B. Jeziorski, “QED calculation of the dipole polarizability of helium atom,” *Phys. Rev. A* **101**, 022505 (2020).
- ¹³P. Czachorowski, M. Przybytek, M. Lesiuk, M. Puchalski, and B. Jeziorski, “Second virial coefficients for ^4He and ^3He from an accurate relativistic interaction potential,” *Phys. Rev. A* **102**, 042810 (2020).

- ¹⁴W. Cencek, J. Komasa, and K. Szalewicz, “Collision-induced dipole polarizability of helium dimer from explicitly correlated calculations,” *J. Chem. Phys.* **135**, 014301 (2011).
- ¹⁵G. Garberoglio and A. H. Harvey, “Path-integral calculation of the second dielectric and refractivity virial coefficients of helium, neon, and argon,” *J. Res. Natl. Inst. Stand. Technol.* **125**, 125022 (2020).
- ¹⁶G. Garberoglio, A. H. Harvey, and B. Jeziorski, “Path-integral calculation of the third dielectric virial coefficient of noble gases,” *J. Chem. Phys.* **155**, 234103 (2021).
- ¹⁷J. Lang, M. Przybytek, M. Lesiuk, and B. Jeziorski, “Collision-induced three-body polarizability of helium,” *J. Chem. Phys.* **158**, 114303 (2023).
- ¹⁸J. Lang, G. Garberoglio, M. Przybytek, M. Jeziorska, and B. Jeziorski, “Three-body potential and third virial coefficients for helium including relativistic and nuclear-motion effects,” *Phys. Chem. Chem. Phys.* **25**, 23395 (2023).
- ¹⁹S. F. Boys and F. Bernardi, “The calculation of small molecular interactions by the differences of separate total energies. Some procedures with reduced errors,” *Mol. Phys.* **19**, 553–566 (1970).
- ²⁰M. Gutowski, J. H. Van Lenthe, J. Verbeek, F. B. Van Duijn-eveldt, and G. Chalasinski, “The basis set superposition error in correlated electronic structure calculations,” *Chem. Phys. Lett.* **124**, 370–375 (1986).
- ²¹G. Chalasinski and M. M. Szczesniak, “State of the art and challenges of the *ab initio* theory of intermolecular interactions,” *Chem. Rev.* **100**, 4227–4252 (2000).
- ²²B. Skwara, W. Bartkowiak, and D. L. Silva, “On the Basis Set Superposition Error in Supermolecular Calculations of Interaction-Induced Electric Properties: Many-Body Components,” *Theor. Chim. Acta* **122**, 127–136 (2009).
- ²³K. Hald, F. Pawłowski, P. Jørgensen, and C. Hättig, “Calculation of frequency-dependent polarizabilities using the approximate coupled-cluster triples model CC3,” *J. Chem. Phys.* **118**, 1292–1300 (2003).
- ²⁴K. Aidas, C. Angeli, K. L. Bak, V. Bakken, R. Bast, L. Boman, O. Christiansen, R. Cimiraglia, S. Coriani, P. Dahle, *et al.*, “The Dalton quantum chemistry program system,” *Wiley Interdiscip. Rev.: Comput. Mol. Sci.* **4**, 269–284 (2014).
- ²⁵“Dalton, a molecular electronic structure program, release 2018,” (2018), see <https://daltonprogram.org>.
- ²⁶W. Cencek, M. Przybytek, J. Komasa, J. B. Mehl, B. Jeziorski, and K. Szalewicz, “Effects of adiabatic, relativistic, and quantum electrodynamics interactions on the pair potential and thermophysical properties of helium,” *J. Chem. Phys.* **136**, 224303 (2012).
- ²⁷T. H. Dunning, “Gaussian basis sets for use in correlated molecular calculations. I. The atoms boron through neon and hydrogen,” *J. Chem. Phys.* **90**, 1007–1023 (1989).
- ²⁸D. E. Woon and T. H. Dunning, “Gaussian basis sets for use in correlated molecular calculations. IV. Calculation of static electrical response properties,” *J. Chem. Phys.* **100**, 2975–2988 (1994).
- ²⁹X. Li and K. L. C. Hunt, “Nonadditive three-body dipoles of inert gas trimers and $\text{H}_2\cdots\text{H}_2\cdots\text{H}_2$: Long-range effects in far infrared absorption and triple vibrational transitions,” *J. Chem. Phys.* **107**, 4133–4153 (1997).
- ³⁰K. T. Tang and J. P. Toennies, “An improved simple model for the van der Waals potential based on universal damping functions for the dispersion coefficients,” *J. Chem. Phys.* **80**, 3726–3741 (1984).
- ³¹L. W. Bruch, C. T. Corcoran, and F. Weinhold, “On the dipole moment of three identical spherical atoms,” *Mol. Phys.* **35**, 1205–1210 (1978).
- ³²P. W. Fowler, “Dispersion dipoles, quadrupoles and electric-field gradients,” *Chem. Phys.* **143**, 447–457 (1990).
- ³³D. M. Bishop and J. Pipin, “Calculation of the dispersion-dipole coefficients for interactions between H, He, and H_2 ,” *J. Chem. Phys.* **98**, 4003–4008 (1993).
- ³⁴D. M. Whisnant and W. Byers Brown, “Dispersion dipole be-

- tween rare-gas atoms,” *Mol. Phys.* **26**, 1105–1119 (1973).
- ³⁵P. H. Martin, “The long-range dipole moment of three identical atoms,” *Mol. Phys.* **27**, 129–134 (1974).
- ³⁶P. Virtanen, R. Gommers, T. E. Oliphant, M. Haberland, T. Reddy, D. Cournapeau, E. Burovski, P. Peterson, W. Weckesser, J. Bright, S. J. van der Walt, M. Brett, J. Wilson, K. J. Millman, N. Mayorov, A. R. J. Nelson, E. Jones, R. Kern, E. Larson, C. J. Carey, Í. Polat, Y. Feng, E. W. Moore, J. VanderPlas, D. Laxalde, J. Perktold, R. Cimrman, I. Henriksen, E. A. Quintero, C. R. Harris, A. M. Archibald, A. H. Ribeiro, F. Pedregosa, P. van Mulbregt, and SciPy 1.0 Contributors, “SciPy 1.0: Fundamental Algorithms for Scientific Computing in Python,” *Nat. Methods* **17**, 261–272 (2020).
- ³⁷D. M. Ceperley, “Path integrals in the theory of condensed helium,” *Rev. Mod. Phys.* **67**, 279 (1995).
- ³⁸R. P. Feynman and A. R. Hibbs, *Quantum Mechanics and Path Integrals* (McGraw-Hill, New York, 1965).
- ³⁹G. Garberoglio and A. H. Harvey, “Path-integral calculation of the third virial coefficient of quantum gases at low temperatures,” *J. Chem. Phys.* **134**, 134106 (2011), Erratum. *J. Chem. Phys.* **152** 199903 (2020).
- ⁴⁰G. Garberoglio and A. H. Harvey, “First-principles calculation of the third virial coefficient of helium,” *J. Res. Nat. Inst. Stand. Technol.* **114**, 249–262 (2009).
- ⁴¹G. Garberoglio, M. R. Moldover, and A. H. Harvey, “Improved first-principles calculation of the third virial coefficient of helium,” *J. Res. Nat. Inst. Stand. Technol.* **116**, 729–742 (2011), Erratum: *J. Res. Nat. Inst. Stand. Technol.* **125** 125019 (2020).
- ⁴²L. D. Fosdick and H. F. Jordan, “Path-integral calculation of the two-particle Slater sum for He⁴,” *Phys. Rev.* **143**, 58 (1966).
- ⁴³H. F. Jordan and L. D. Fosdick, “Three-particle effects in the pair distribution function for He⁴ gas,” *Phys. Rev.* **171**, 128 (1968).
- ⁴⁴G. Garberoglio and A. H. Harvey, “Path-integral calculation of the fourth virial coefficient of helium isotopes,” *J. Chem. Phys.* **154**, 104107 (2021).
- ⁴⁵S. Kirouac and T. K. Bose, “Polarizability and dielectric properties of helium,” *J. Chem. Phys.* **64**, 1580–1582 (1976).
- ⁴⁶M. Lallemand and D. Vidal, “Variation of the polarizability of noble gases with density,” *J. Chem. Phys.* **66**, 4776–4780 (1977).
- ⁴⁷J. Huot and T. K. Bose, “Experimental determination of the dielectric virial coefficients of atomic gases as a function of temperature,” *J. Chem. Phys.* **95**, 2683–2687 (1991).
- ⁴⁸C. Gaiser and B. Fellmuth, “Highly-accurate density-virial-coefficient values for helium, neon, and argon at 0.01 °C determined by dielectric-constant gas thermometry,” *J. Chem. Phys.* **150**, 134303 (2019).
- ⁴⁹D. Binosi, G. Garberoglio, and A. H. Harvey, “Third density and acoustic virial coefficients of helium isotopologues from *ab initio* calculations,” *J. Chem. Phys.* **160**, 244305 (2024).
- ⁵⁰M. P. White and D. Guggan, “Direct measurements of the dielectric virial coefficients of ⁴He between 3 K and 18 K,” *Metrologia* **29**, 37–57 (1992).